Cerocene Revisited: The Electronic Structure of and Interconversion Between $Ce_2(C_8H_8)_3$ and $Ce(C_8H_8)_2$

*Marc D. Walter, Corwin H. Booth, Wayne W. Lukens, and Richard A. Andersen**

Department of Chemistry and Chemical Sciences Division of Lawrence Berkeley National Laboratory, University of California, Berkeley, California 94720

E-mail: raandersen@lbl.gov

RECEIVED DATE (to be automatically inserted after your manuscript is accepted if required according to the journal that you are submitting your paper to)

To whom correspondence should be addressed. E-mail: raandersen@lbl.gov

Abstract

New synthetic procedures for the preparation of $Ce(cot)_2$, cerocene, from $[Li(thf)_4][Ce(cot)_2]$, and $Ce_2(cot)_3$ in high yield and purity are reported. Heating solid $Ce(cot)_2$ yields $Ce_2(cot)_3$ and COT while heating $Ce_2(cot)_3$ with an excess of COT in C_6D_6 to 65 °C over four months yields $Ce(cot)_2$. The solid state magnetic susceptibility of these three organocerium compounds shows that $Ce(cot)_2$ behaves as a TIP (temperature independent paramagnet) over the temperature range of 5-300 K, while that of $Ce_2(cot)_3$ shows that the spin carriers are antiferromagnetically coupled below 10 K; above 10 K, the individual spins are uncorrelated, and $[Ce(cot)_2]^-$ behaves as an isolated f^1 paramagnet. The EPR at 1.5 K for $Ce_2(cot)_3$ and $[Ce(cot)_2]^-$ have ground state of $M_J = \pm 1/2$. The L_{III} edge XANES of $Ce(cot)_2$ (Booth, C.H.; Walter, M.D.; Daniel, M.; Lukens, W.W., Andersen, R.A., *Phys. Rev. Lett.* **2005**, *95*, 267202) and

$Ce_2(cot)_3$ over 30-500 K are reported; the $Ce(cot)_2$ XANES spectra show Ce(III) and Ce(IV) signatures up to a temperature of approximately 500 K, whereupon the Ce(IV) signature disappears, consistent with the thermal behavior observed in the melting experiment. The EXAFS of $Ce(cot)_2$ and $Ce_2(cot)_3$ are reported at 30 K; the agreement between the molecular parameters for $Ce(cot)_2$ derived from EXAFS and single crystal X-ray diffraction data are excellent. In the case of $Ce_2(cot)_3$ no X-ray diffraction data are known to exist, but the EXAFS are consistent with a "triple-decker" sandwich structure. A molecular rationalization is presented for the electronic structure of cerocene having a multiconfiguration ground state that is an admixture of the two configurations Ce(III, $4f^1$)($cot^{1.5-}$)$_2$ and Ce(IV, $4f^0$)(cot^{2-})$_2$; the multiconfigurational ground state has profound effects on the magnetic properties and on the nature of the chemical bond in cerocene and, perhaps, other molecules.

Introduction

The initial synthesis of cerocene, Ce(η^8-C_8H_8)$_2$ or $Ce(cot)_2$, over thirty years ago,[1] caused little excitement or controversy since it was assumed to be the lanthanide analogue of thorocene and uranocene, both of which were known.[1, 2] These cot-derivatives were formulated as being derived from two cyclooctatraene dianions, each of which contain 10 π-electrons and therefore are Hückel aromatic, which resulted in an oxidation number of four assigned to the metal atoms in these sandwich molecules, that is, the electronic structure of cerocene was expected to be Ce(IV, $4f^0$)(cot^{2-})$_2$. This formulation is supported by ionic radii sum arguments and by the apparent diamagnetism as judged by the ^{1}H NMR spectrum.[1, 3] Further support was derived from gas phase photoelectron spectroscopic studies which showed that the He(I) and He(II) spectra are superimposable on those of $Th(cot)_2$.[3, 4] This simple and comfortable view of the bonding was challenged by quantum mechanical calculations at the intermediate neglect of differential overlap (INDO) level of theory in which the cerium ion was treated as a point charge, reported in 1989 by Neumann and Fulde.[5] These authors postulated that the electronic configuration Ce(III, $4f^1$)($cot^{1.5-}$) was lower in energy than that of Ce(IV, $4f^0$)(cot^{2-})$_2$ and that the ground state is an orbital singlet, and that the magnetic susceptibility of cerocene should show temperature

independent paramagnetism, $\chi_m > 0$, rather than diamagnetism, $\chi_m < 0$. The initial calculations were supported by high level multireference configuration interaction including single and double excitation (MRCISD) studies which predict that the ground state is an admixture of the two wave functions represented by Ce(III, $4f^1$)($cot^{1.5-}$)$_2$ and Ce(IV, $4f^0$)(cot^{2-})$_2$.[6-9] Early experimental evidence supporting this hypothesis was provided by room temperature Ce K-edge X-ray absorption near edge (XANES) spectra of substituted cerocene derivatives, [1,4-$(Me_3Si)_2C_8H_6$]$_2$Ce and [1,3,6-$(Me_3Si)_3C_8H_5$]$_2$Ce, indicating that the K-edge position lies in the range found for various Ce(III) model compounds,[10] and more recently by absorption, MCD and luminescence spectra on [1,4-$(Me_3Si)_2C_8H_6$]$_2$Ce at variable temperatures, which are more consistent with a Ce(III) compound.[11] We have recently published high resolution Ce L_{III}-edge XANES as a function of temperature; this study along with variable temperature magnetic susceptibility data support the model that the ground state of cerocene is multiconfigurational and not diamagnetic as χ_m is positive and temperature independent (TIP).[12] These physical studies required a high-purity synthesis of Ce(cot)$_2$, which was not available.

This paper describes a convenient synthesis of Ce(cot)$_2$ and $Ce_2(cot)_3$. In addition, their molecular structures are determined using the local structure extended X-ray absorption fine-structure (EXAFS) technique, providing the first evidence of the triple-decker structure of $Ce_2(cot)_3$. The Ce L_{III} edge of cerocene as a function of temperature provides experimental evidence for the multiconfiguration ground state advocated by the calculational studies.[6-9]

Results and Discussion

Previous synthetic studies. The initial synthesis of K[Ce(cot)$_2$] used K_2cot and $CeCl_3$ in tetrahydrofuran.[13] In our hands, this synthesis method did not produce useable quantities of K[Ce(cot)$_2$]. Although a synthetic route from CeI_3 and K_2cot has recently been published, a difficulty is that K[Ce(cot)$_2$] does not have an ^{1}H NMR spectrum at room temperature in either thf-d_8 or pyridine-d_5 and the anion is insoluble in C_6D_6. Thus, the purity of the anion is not readily determined. The lithium and sodium salts of the cerate, [Li(thf)$_4$][Ce(cot)$_2$] and [Na(thf)$_3$][Ce(cot)$_2$], have been prepared, and more

importantly, these complexes display ^{1}H NMR resonances.[14] The potassium salt of the cerate is an important reagent since $Ce(cot)_2$ is prepared from it by oxidation with AgI or allyl bromide.[3, 15] Alternatively, cerocene can be prepared from $Ce(O\text{-}i\text{-}Pr)_4 \bullet i\text{-}PrOH$, C_8H_8 and Et_3Al.[1] However, this synthetic route requires large quantities of C_8H_8 as reagent and solvent, which is now very expensive. Since studies of the physical properties outlined in the Introduction require reasonable quantities of $Ce(cot)_2$ in high purity, a good salt metathesis route is clearly desirable; a synthetic route is described below.

Synthesis and Physical Properties of $[Li(thf)_4][Ce(cot)_2]$. $Li_2(cot)$ is prepared from Li-wire and cyclooctatetraene in tetrahydrofuran and purified by crystallization from that solvent. The light green crystals contain coordinated solvent, and its stoichiometry may be determined by integration of the ^{1}H NMR spectrum in pyridine-d_5. Anhydrous $CeCl_3$ reacts cleanly with two equivalents of $Li_2(cot)$ in boiling tetrahydrofuran to give a deep green solution, from which $[Li(thf)_4][Ce(cot)_2]$ may be crystallized as exceedingly air sensitive, green needles in good yield, eq. 1.

$$2\,[Li(thf)_x]_2(C_8H_8) + CeCl_3 \xrightarrow[-\,3\,LiCl,\,66\,\%]{THF} [Li(thf)_4][Ce(C_8H_8)_2] \qquad (1)$$

The physical properties of the anion are identical to those previously reported,[14] with the exception of the ^{1}H NMR spectrum. The cerate is insoluble in C_6D_6 and the ^{1}H NMR spectra are obtained in either thf-d_8 or pyridine-d_5 in which the C_8H_8 resonances are observed at 20 °C at δ 1.50 ($\nu_{1/2}$ = 100 Hz) or δ 2.44 ($\nu_{1/2}$ = 130 Hz), respectively, in addition to resonances at δ 1.6 and 3.5 due to thf-d_0. The resonance due to the cot ligand is temperature dependent as expected for a paramagnetic compound, and the δ vs. T^{-1} plot is shown in Figure 1; the resonances due to thf are nearly temperature independent and they are shifted upfield relative to those of free thf by ca. 0.1 ppm. The reported ^{1}H NMR spectrum in thf-d_8

contains two resonances at δ 0.34 and 0.04;[14] these two resonances have never been observed in any of our spectra, and we do not know their identity.

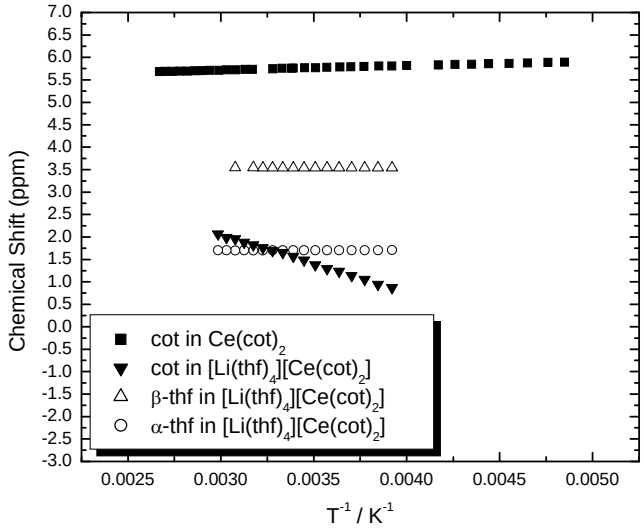

Figure 1. Chemical shift (δ) vs. T^{-1} plots of $[Li(thf)_4][Ce(cot)_2]$ in thf-d_8 and of $Ce(cot)_2$ in toluene-d_8. The low solubility of $[Li(thf)_4][Ce(cot)_2]$ limited the accessible temperature regime to 255-355 K, whereas the ^{1}H NMR spectra for $Ce(cot)_2$ were collected from 206 to 375 K.

Solid State Magnetism (SQUID) of $[Li(thf)_4][Ce(cot)_2]$. The reported magnetic moment of $K[Ce(cot)_2]$ in tetrahydrofuran solution of 1.88 μ_B (at 300 K)[13] is thought to be incorrect, since cerium(III) is a $4f^1$ ion and the free ion term is ^2F with a magnetic moment of 2.54 Bohr magnetons (μ_B).[16-18] Spin-orbit coupling splits this state into two levels with J= 5/2 (ground state) and J= 7/2 (excited state) with a separation in the free ion of ca. 2200 cm^{-1}, so the J= 7/2 state is not populated at 293 K (kT= 205 cm^{-1}). The crystal field splits the ground state into three Kramer's doublets with M_J=±1/2, ±3/2, and ±5/2, which are more conveniently represented using the $|J,M_J>$ representation. Thus, the three Kramers doublets are |5/2, ±1/2>, |5/2,±3/2> and |5/2,±5/2>. These states are populated thermally according to the Boltzmann distribution, resulting in a χ^{-1} vs. T plot that is non-linear, *i.e.*, it deviates from the Curie-Weiss law, $\chi^{-1} = C/(T-\theta)$. The solid state magnetic susceptibility study on

$[Li(thf)_4][Ce(cot)_2]$ was performed as previously reported,[19] and an effective magnetic moment of 2.21 μ_B at 300 K is observed (Figure 2). This value is in good agreement with the limiting value of 2.14 μ_B predicted by Warren.[16, 17]

At T< 200 K, the plot of χT vs. T is linear with a sharp deviation at T< 10 K. The reason for the non-linear behavior at low T is unknown but is assumed to be due to intermolecular antiferromagnetic interactions. The linear behavior of the χT vs. T is caused by mixing of a thermally isolated ground (M_J) state with a low-lying but thermally unpopulated excited state with $\Delta M_J = \pm 1$ resulting in strong second-order Zeeman effects. The value of μ_{eff} for the ground state, 1.77 μ_B, may be determined by extrapolating χT to 0 K ($\mu_{eff}^2 = 7.997\ \chi T$).

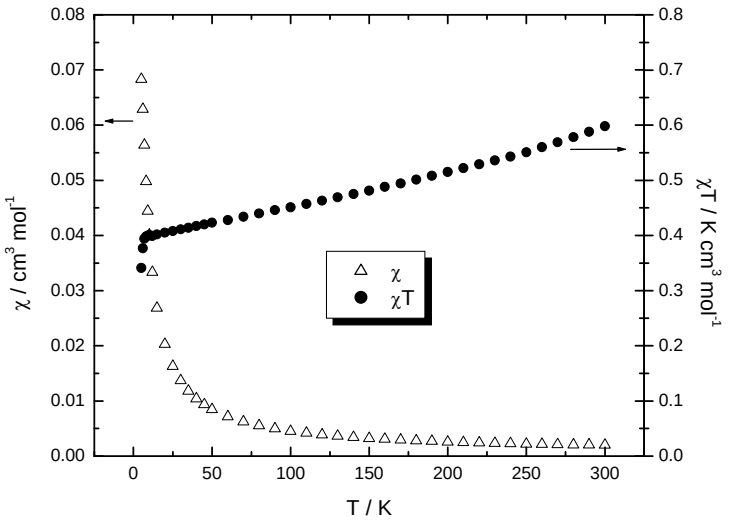

Figure 2. χ (triangles) and χT (circles) vs. T plots for $[Li(thf)_4][Ce(cot)_2]$ at 0.5 T.

Electron Paramagnetic Resonance (EPR) spectrum and ground state of $[Li(thf)_4][Ce(cot)_2]$. The EPR spectrum and its simulation for $[Li(thf)_4][Ce(cot)_2]$ is shown in Figure 3. The g-values derived from fitting the spectrum are g_1= 2.270, g_2 = 2.274, and g_3 = 1.123. Since $4\mu_{eff}^2 = g_1^2 + g_2^2 + g_3^2$, μ_{eff} derived from the EPR spectrum is 1.70 μ_B in good agreement with the value of 1.77 μ_B obtained from the SQUID measurements, which strongly supports the assertion that the state observed by EPR is

indeed the ground state. The g-values obtained by fitting the spectrum describe an axial complex with $g_{\perp} = 2.272$ and $g_{\parallel} = 1.123$.

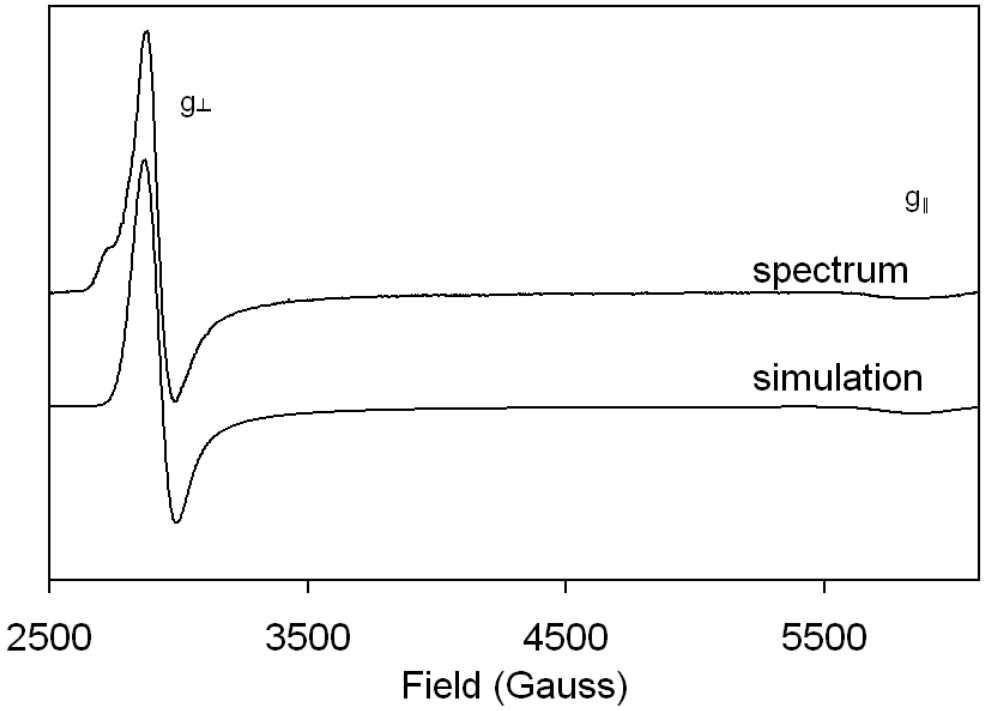

Figure 3. EPR spectrum and simulation for $[Li(thf)_4][Ce(cot)_2]$ at 1.5 K, $g_{\perp} = 2.272$ and $g_{\parallel} = 1.123$.

As noted above, the ground state of Ce(III) is J=5/2, which is split by the crystal field into three Kramers's doublets: |5/2,±1/2>, |5/2,±3/2>, and |5/2,±7/2>. Each of these doublets has a characteristic EPR spectrum given by the following:[20]

|5/2,±1/2>: $g_{\parallel} = 6/7 = 0.86$, $g_{\perp} = 18/7 = 2.57$

|5/2,±3/2>: $g_{\parallel} = 18/7 = 2.57$, $g_{\perp} = 0$

|5/2,±5/2>: $g_{\parallel} = 30/7 = 4.29$, $g_{\perp} = 0$.

The observed g-values are close to those for $M_J = \pm 1/2$, so the ground state of $[Li(thf)_4][Ce(cot)_2]$ must largely consist of |5/2,±1/2>. The disagreement between the observed g-values and those of |5/2,±1/2> are due to either mixing of |5/2,±3/2> and/or |5/2,±5/2> with |5/2,±1/2> or are due to mixing with the excited J=7/2 state, especially |7/2,±1/2>.[21] Since an axial crystal field with symmetry C_n mixes states of $M_J = \pm n$, no mixing of the different M_J levels for $[Li(thf)_4][Ce(cot)_2]$ with D_{8h} idealized

symmetry is expected.[20] In reality, the site symmetry of $[Li(thf)_4][Ce(cot)_2]$ is only C_2, so mixing of the M_J levels is possible but will not be large as the local symmetry is very close to C_8. A more likely explanation is mixing of $|7/2,\pm1/2\rangle$ with the ground state producing a ground state of the form $\pm a|5/2,\pm1/2\rangle \pm b|7/2,\pm1/2\rangle$, where $a^2 + b^2 = 1$. The best fit to the observed g-values yields a = 0.990 and b = 0.143, which yields $g_{\|}$(calc.) = 1.143 and $g_{\perp}$(calc.) = 2.285 in good agreement with the observed values of 1.123 and 2.272, respectively. Including an orbital reduction factor, k, to account for the small amount of covalence in this complex gives an exact fit to the data with a = 0.991, b = 0.131, and k = 0.990.

The primarily $|5/2,\pm1/2\rangle$ ground state of $[Li(thf)_4][Ce(cot)_2]$ may be more clearly represented using $|M_l,M_S\rangle$ rather than $|J,M_J\rangle$ to better illustrate the interaction between the cot^{2-} ligand and Ce atomic orbitals. As previously shown by Gourier, $\pm|5/2, 1/2\rangle$ in $|J,M_J\rangle$ can be transformed to $\pm0.65|0,1/2\rangle \pm 0.76|1,1/2\rangle$ in $|M_l,M_S\rangle$;[22] in other words, the unpaired electron in $\pm|5/2, 1/2\rangle$ has approximately equal f_z^3 and (f_{zx}^2, f_{yz}^2) character (Table 1). This observation may seem counterintuitive as the ($f_{x(x^2-3y^2)}$, $f_{y(3x^2-y^2)}$) orbitals have the correct symmetry to interact with the lowest lying unoccupied orbitals of the cot^{2-} ligands although the overlap is expected to be small. The implicit assumption that makes the orbital energy ordering seem counterintuitive is that the Ce 4f orbitals are an appropriate basis from which to examine bonding with the ligand orbitals. However, spin-orbit coupling is expected to be significantly larger than the bonding interactions between the cot^{2-} ligands and the Ce(III) center;[20, 21] therefore, the J=5/2 states and not the 4f orbitals are the appropriate basis. In $[Li(thf)_4][Ce(cot)_2]$, as in $U(C_7H_7)_2^-$, only the f_{xyz} and $f_{(x^2-y^2)z}$ orbitals have the proper symmetry and sufficient overlap to interact strongly with the ligands, which makes the orbital ordering easily understood, The orbitals most destabilized by interaction with the filled ligand orbitals are those with the most f_{xyz} and $f_{(x^2-y^2)z}$ character. Therefore, $|5/2, \pm3/2\rangle$ will be most destabilized, and $|5/2. \pm1/2\rangle$ will be lowest in energy as observed. The orbital that will be most stabilized by interaction with the empty ligand orbitals, ($f_{x(x^2-3y^2)}$, $f_{y(3x^2-y^2)}$), belongs to the J=7/2 state with M_J=7/2 and is destabilized by ~2200 cm^{-1} relative to the J=5/2 states due to spin-orbit coupling.

Table 1. Composition of the *J*=5/2 ground state in terms of the 4f states[22]

J=5/2 state	f_{z^3} (%) f_σ	(f_{xz^2}, f_{yz^2})(%) f_π	f_{xyz} , $f_{(x^2-y^2)z}$ (%) f_δ	$f_{x(x^2-3y^2)}, f_{y(3x^2-y^2)}$(%) f_φ
|5/2. ±1/2>	42.9	57.1		
|5/2, ±3/2>		28.6	71.4	
|5/2, ±5/2>			14.2	85.8

Oxidation of [Li(thf)$_4$][Ce(cot)$_2$] to give Ce(cot)$_2$. The synthesis of [Li(thf)$_4$][Ce(cot)$_2$] provides a convenient starting material in high purity, and various oxidizing reagents for the preparation of cerocene are investigated. In our hands, [Cp_2Fe][PF_6] in tetrahydrofuran or *p*-benzoquinone (ratio 1:1) in toluene oxidize the cerate cleanly (Scheme 1).[23] These two reagents are excellent oxidizing reagents in cerium chemistry.[24]

Scheme 1.

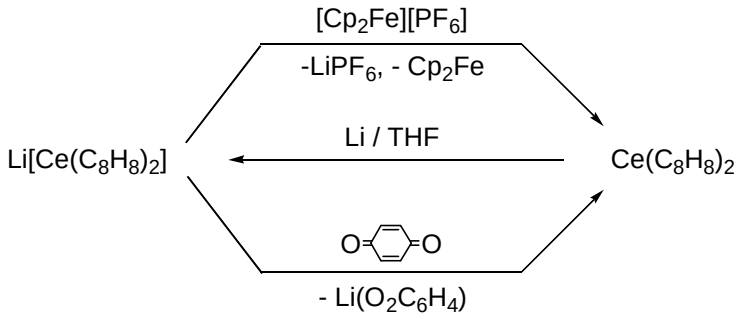

A complete conversion of Li[Ce(cot)$_2$] is not achieved with 1:0.5 ratio of *p*-benzoquinone. The facility of this oxidation is demonstrated by the fact that Li[Ce(cot)$_2$] reacts with *p*-benzoquinone even in the solid state as indicated by a color change from light green to deep purple-red, when the two

reactants are mixed in a flask before solvent is added. Cerocene, $Ce(cot)_2$, is obtained by continuous extraction with boiling toluene,[25] from which it crystallizes in moderate yield and high purity, as dark red needles, sparingly soluble in aromatic hydrocarbons and tetrahydrofuran. The absence of lithium containing by-products was verified by a negative flame test. In the solid state it inflames immediately in the presence of oxygen. Its physical properties are as previously reported.[1, 3, 15] The ^{1}H and $^{13}C\{^{1}H\}$ NMR spectra of cerocene in C_6D_6 as solvent consist of a single sharp resonance at 5.79 ppm (^{1}H) and 114.9 ppm (^{13}C), and the ^{1}H NMR chemical shift shows only a small temperature dependence (Figure 1).

Although a molecular ion with the correct isotope pattern is observed in the EI mass spectrum for $Ce(cot)_2$, it does not sublime in diffusion pump vacuum, in sharp contrast to $Th(C_8H_8)_2$ and $U(C_8H_8)_2$;[26, 27] instead it decomposes, see below. This is rather surprising considering that powder diffraction data suggested that $Ce(C_8H_8)_2$ is isostructural and isomorphous to $Th(C_8H_8)_2$ and $U(C_8H_8)_2$;[1] a single crystal X-ray structure has recently appeared, and $Ce(cot)_2$ is indeed isomorphous with $Th(C_8H_8)_2$ and $U(C_8H_8)_2$.[28] The unexpected lack of volatility observed for $Ce(cot)_2$ compared to its uranium and thorium analogues warranted further investigations of its thermal properties; see below.

Solid State Magnetism (SQUID) of $Ce(cot)_2$. The temperature dependence of the magnetic susceptibility is shown in Figure 4 as χ and χT vs. T plots. In the published χ vs. T plot, the diamagnetic contribution from the C_8H_8 rings is removed using Pascal´s constants.[12] In Figure 4, the diamagnetic contribution is removed using the published high-temperature data (50-300 K) for thorocene, which is diamagnetic.[29] The TIP value of $1.7(2) \times 10^{-4}$ emu/mol compares well with the published value of $1.4(2) \times 10^{-4}$ emu/mol using Pascal´s constants.

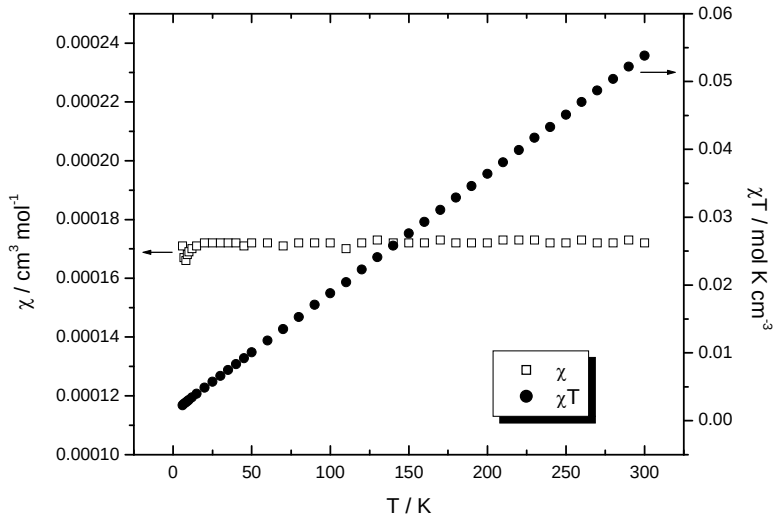

Figure 4. χ and χT vs. T plots for $Ce(cot)_2$.

Thermal conversion of $Ce(cot)_2$ to $Ce_2(cot)_3$. Unlike $Th(cot)_2$, which sublimes at 135-160 °C in vacuum,[27, 30, 31] and $U(cot)_2$, which sublimes at 140-210 °C in vacuum,[26, 32, 33] cerocene does not sublime when heated under diffusion pump vacuum. Instead, a red film forms on the cold walls of the sublimator when heated rapidly in vacuum,[25] while most of the material formed a green powder insoluble in all common organic solvents. This unusual temperature behavior was investigated in the following way. When cerocene is heated in a melting point capillary, sealed under nitrogen, the solid did not melt but changed color from dark red to green and a yellow liquid formed in the head space at 290-292 °C.[31] Opening the capillary and examining the volatile material by ^{1}H NMR spectroscopy shows it to be free C_8H_8. The insoluble green powder was identified by IR spectroscopy as $Ce_2(cot)_3$.[1] Thus, the clean thermal decomposition of cerocene provides an excellent synthesis of the dicerium triple-decker sandwich compound, eq. 2. It is noteworthy that storage of $Ce(cot)_2$ in a glass ampoule at room temperature in the dark for 140 weeks also resulted in formation of $Ce_2(cot)_3$ (ca. 10 %, an estimate based on magnetic susceptibility measurements). The reverse process is achieved by suspending $Ce_2(cot)_3$ in a ca. 70-fold excess of C_8H_8 in C_6D_6 at 65 °C and monitoring the ^{1}H NMR spectrum. Over a time span of 4 months, the formation of $Ce(cot)_2$ is complete. In the presence of catalytic amounts of

$Al(C_2H_5)_3$ and a 70-fold excess of COT at 130 °C, the conversion is complete within 1 h.[1] The rate difference may be explained by the insolubility of $Ce_2(cot)_3$ in C_6D_6 at 65 °C. The thermal behavior is similar to that of $Ti_2(C_8H_8)_3$.[34]

$$2\ Ce(C_8H_8)_2 \rightleftharpoons Ce_2(C_8H_8)_3 + C_8H_8 \qquad (2)$$

The original synthesis reported by Greco and co-workers is shown in Scheme 2. It seems reasonable to suggest that $Ce_2(cot)_3$ is formed along with $Ce(cot)_2$ but it is rapidly converted to cerocene under the conditions employed, *i.e.*, with C_8H_8 acting as reactant and solvent.[1] Alternatively, this molecule has been prepared by co-condensation of cerium metal atoms and C_8H_8 at –196 °C.[35]

Scheme 2. Synthesis of $Ce(cot)_2$ and $Ce_2(cot)_3$.[1]

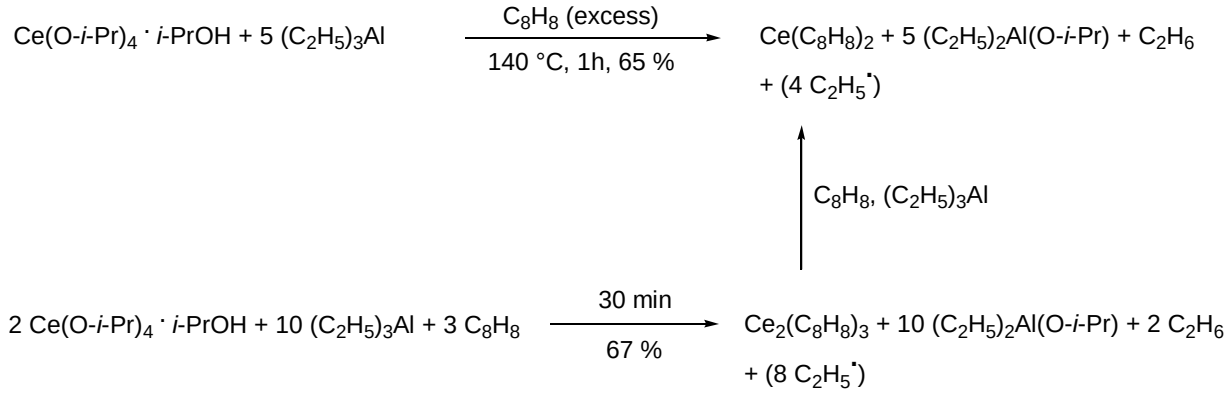

EPR Spectrum and ground state of $Ce_2(cot)_2$. As shown in Figure 5, $Ce_2(cot)_3$ has the characteristic spectrum of a spin triplet state with axial symmetry, which is clearly indicated by the present of the half-field peak with g=4.83.[20] The zero-field splitting of $g_\perp$ disappears as the sample temperature is increased above ~3 K, presumably due to exchange narrowing (see Supporting Information, Figure S1).[36] The ground state of $Ce_2(cot)_3$ is very similar to that of $[Li(thf)_4][Ce(cot)_2]$ and has similar g values: $g_\perp = 2.335$ and $g_\parallel = 0.974$. Using the approach described above, the ground state for $Ce_2(cot)_3$ is $\pm a|5/2,\pm1/2\rangle \pm b|7/2,\pm1/2\rangle$, with a= 0.999, b= 0.051, and k= 0.967, which yields g-values identical to

the observed ones. Like the g-values, the zero-field splitting (ZFS) for this system is anisotropic with $|D_{\|}| = 0.020$ cm^{-1} and $|D_{\perp}| = 0.014$ cm^{-1}, which is not surprising as the anisotropy in g makes the ZFS due to both dipole-dipole coupling and exchange coupling anisotropic.[36]

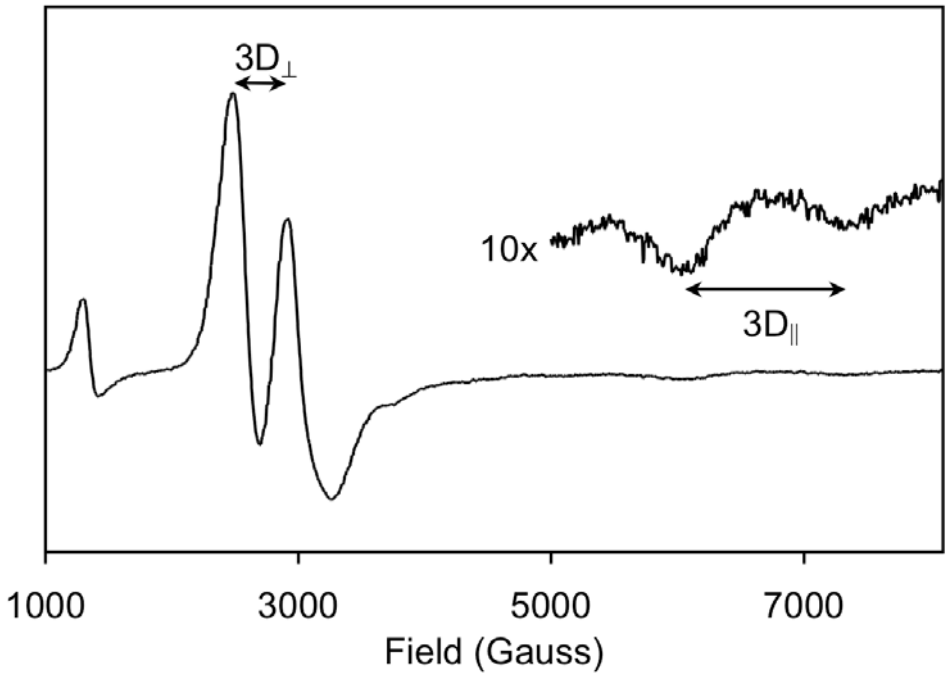

Figure 5. EPR spectrum of $Ce_2(cot)_3$ at 1.5 K, $g_{\|} = 0.974$, $g_{\perp} = 2.335$, $|D_{\|}| = 0.020$ cm^{-1} and $|D_{\perp}| = 0.014$ .cm^{-1}

Solid State Magnetism (SQUID) of $Ce_2(cot)_3$. The magnetic properties of the triple-decker complex were determined in order to explore the question of exchange coupling across the cot^{2-} ligand. The paramagnetic cerium(III), f^1, spin carriers are separated by about 4 Å, as estimated from the EXAFS data, see below. The solid state magnetic susceptibility was recorded from 2-300 K, see Figure 6. At high temperature, the $1/\chi$ vs. T plot is as expected for two uncorrelated spin carriers and yields an effective magnetic moment of 2.8 μ_B per molecule (2.0 μ_B per Ce(III) center) at 300 K. At low temperature, the value of χ increases normally with decreasing temperature until a maximum is reached

and then declines rapidly with decreasing temperature. This behavior is indicative of antiferromagnetic spin exchange interaction, and the temperature at which the maximum susceptibility occurs is the Néel temperature (T_N), which occurs at 8 K (Figure 6).

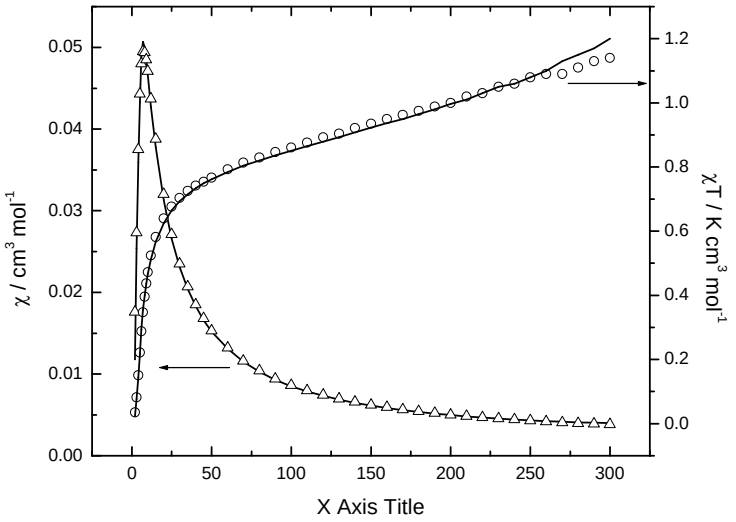

Figure 6. Magnetic susceptibility (triangles) and χT (circles) of $Ce_2(cot)_3$ at 4 T. The fit of the data to eq. 4 with J'/k = -3.2 K is shown in the solid lines.

The susceptibility may be modeled using the approach developed by Lines for modeling coupling between two ions with unquenched orbital angular momentum.[37] Briefly, the Lines approach treats each ion as an effective spin, $\tilde{\mathbf{S}}$, 1/2 system in which the spins are coupled isotropically (Heisenberg coupling, $\mathcal{H}_{ex}=2J'(\tilde{\mathbf{S}}\bullet\tilde{\mathbf{S}})$). In addition, the g-factor in the usual equation for Heisenberg coupling is replaced by a fictitious, temperature dependent g(T). For a dimetallic system, as we have here, the equation for susceptibility is given by eq. 3, where the symbols have their usual meanings, and J' is the coupling constant for the fictitious S=1/2 system. Although Lines cautions that g(T) is not the same as that due to an isolated ion due to exchange splitting of the higher energy states, in the case of $Ce_2(cot)_3$, the exchange splitting is weak, and the coordination environment of Ce is likely to that found in $[Li(thf)_4][Ce(cot)_2]$. Therefore, g(T) for $[Li(thf)_4][Ce(cot)_2]$ should be a good model for g(T) for

$Ce_2(cot)_3$, and eq. 3 may be rewritten in a simpler form as eq. 4 where χ_{mono} is the susceptibility of $[Li(thf)_4][Ce(cot)_2]$. As shown in Figure 6, this model provides an excellent fit to the susceptibility of $Ce_2(cot)_3$. As noted above, the susceptibility of $[Li(thf)_4][Ce(cot)_2]$ was not recorded at T<5K, and χ was estimated using the Curie Law fit for 5 K < T < 80 K for use in eq. 4; these points were not used in the fit and are included to illustrate that the fit to the data for $Ce_2(cot)_3$ is very good even when this approximation is made for χ_{mono} at T < 5 K.

$$\chi = \frac{N[g(T)]^2 \mu_B^2}{4kT}\left(\frac{8}{3+e^{-2J'/kT}}\right) \qquad (3)$$

$$\chi = \chi_{mono}\left(\frac{8}{3+e^{-2J'/kT}}\right) \qquad (4)$$

The coupling constant for the true spin system, J, can be determined from J' if the ground state is known since $J'_x = (g_x/g_J)^2(g_J-1)^2J$ and $J'=(1/3)(J_x'+J_y'+J_z')$ where g_J is the Landé g-value.[20] As shown above, the ground state for $Ce_2(cot)_3$ is mainly |5/2,1/2> for which $g_{\|} \approx g_J = 6/7$ and $g_{\perp} \approx 3g_J$. Therefore, J/k is approximately equal to 147J'/19 or -26 K for the coupling of the true spins (as opposed to the effective spins) in $Ce_2(cot)_3$.

A reasonable microscopic explanation for the coupling is a polarization model,[38] which is an electrostatic model introducing spin correlation through polarization, rather than a molecular orbital model based on the interactions through orbitals. It is impossible to decide which model is more appropriate, but the polarization model has the virtue that it is simple to use and understand. It can be applied to this molecule in the following way. In a linear arrangement, Ce(1)-L-Ce(2), where Ce symbolizes the $(C_8H_8)Ce(III)$ fragment and L symbolizes the bridging dianionic $[C_8H_8]^{2-}$ ligand, the spins on the two Ce(III) fragments can be orientated in two ways: Ce(α)···Ce(α) and Ce(α)···Ce(β). Placing the spin-paired bridging group, represented by L(αβ), between the two Ce(III) fragments, four possible arrangements of the four spins will result: α(αβ)α, α(βα)α, α(αβ)β, and α(βα)β. The difference in energy between these microstates is small, and the state with the α(αβ)β orientation is

slightly energetically preferred, since there are two favorable exchange interactions between spins on the Ce(III) fragments with the spins on the bridging ligand. The spins are therefore polarized, with the result that the spin on each Ce(III) is antiferromagnetically aligned below the Néel temperature. According to the Boltzmann distribution, the other spin alignments get populated with increasing temperature, and increases until the populations of each state are equal (Néel temperature). At higher temperatures, the magnetic susceptibility decreases with increasing temperature, since the spins are uncorrelated. A similar polarization model was used to rationalize the antiferromagnetic coupling in $\{[(C_5Me_5)_2Yb(III)]_2(bipyrimidine)\}$[39] and $\{[(MeC_5H_4)_3U]_2(\mu\text{-}1,4\text{-}N_2C_6H_4)\}$[40]

Ce L_{III} edge XANES Results. Although the degree of f-involvement in bonding in most lanthanide compounds is very low due to the strongly localized character of the 4f orbitals, this situation is not necessarily the case in cerium-based compounds. For instance, in the formally tetravalent-cerium compounds CeO_2 and CeF_4, clear features are present in both[41] Ce L_{III} X-ray absorption[42] and X-ray photoelectron spectra that indicate a fractional f-occupancy, n_f, near 0.5. Anderson model calculations[43] agree with these measurements which find that the remaining f-weight is delocalized over the ligands. More recently, we have found that cerium in cerocene is similarly intermediate valent with n_f= 0.89.[12] Figure 7 shows these data together with Ce L_{III} XANES from a $Ce_2(cot)_3$ sample and from the $Ce(cot)_2$ sample after heating to about 565 K. The first (main) peak near 5722 eV is due to a $2p_{3/2}$ electron transition to a 5d excited state in the presence of the $4f^1$ state, that is, a $\overline{2p_{3/2}}\,4f^15d$ final state (trivalent cerium component). The feature in cerocene near 5734 eV is due to a $\overline{2p_{3/2}}\,4f^05d$ final state (tetravalent cerium component). Interestingly, in $Ce_2(cot)_3$, these data show no tetravalent cerium component. All the data show that cerium is trivalent in $Ce_2(cot)_3$. After cerocene was heated to 500 K, the data similarly shows dominant trivalent cerium character. Differences in the main peak height are likely due to differences in the crystal structure of $Ce(cot)_2$ and $Ce_2(cot)_3$. The conversion from $Ce(cot)_2$ to $Ce_2(cot)_3$, which occurred in the melting experiment at 290-292 °C, appears to be time dependent. The

XANES spectra collected a various temperatures clearly indicate that the conversion already occurs at about 400 K, but is complete at 500 K (see Supporting Information for details, Figure S2).

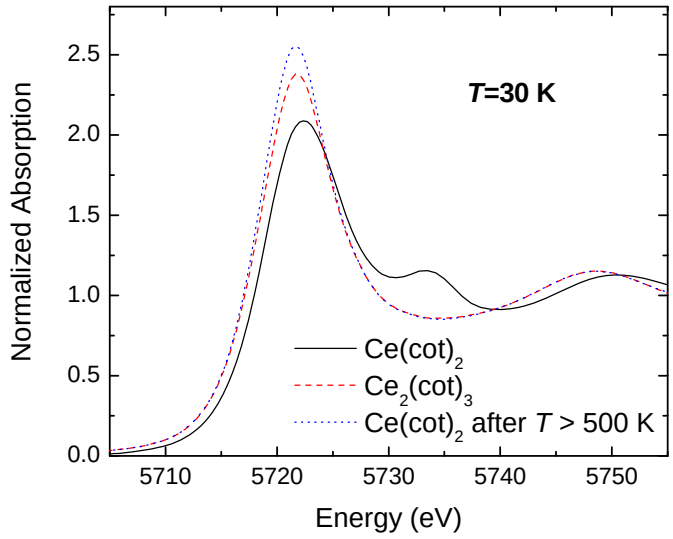

Figure 7. Ce L_{III}-edge X-ray absorption near-edge spectra for $Ce(cot)_2$, $Ce_2(cot)_3$ and $Ce(cot)_2$ after heating to 500 K. The energy is calibrated by placing the first inflection point of the CeO_2 edge at 5723 eV.

Ce L_{III} edge EXAFS Results. Figure 8 shows the $k^2\chi(k)$ data for both the $Ce(cot)_2$ and the $Ce_2(cot)_3$ samples, as well as the cerocene sample that was heated above 500 K. The initial fits to the cerocene data (not shown) are consistent with the known crystal structure, and similar fits to the $Ce_2(cot)_3$ data are consistent with the nominal triple-decker structure. The following results therefore assume the known coordination environment for cerocene, that is, the relative number of neighbors in each scattering shell is constrained to its nominal value. For instance, the number of Ce-H neighbors near 3 Å is constrained to be equal to the number of Ce-C pairs near 2.7 Å. Therefore, deviations from this model are vetted by the bond length distribution variance, σ^2, and the bond length, R, for each peak, and by the overall S_0^2 and ΔE_0 parameters. In addition for the $Ce_2(cot)_3$ fit, we include a single Ce···Ce pair near 4 Å. We include this pair to give a possible measure of the potential Ce···Ce distance, and the fit is

improved by its inclusion. However, we do not claim that this fit is evidence for Ce···Ce scattering, as its inclusion does not pass a Hamilton test. In particular, Ce-C and multiple scattering peaks overlap strongly with the possible Ce···Ce scattering, rendering a reliable measurement impossible with these data.

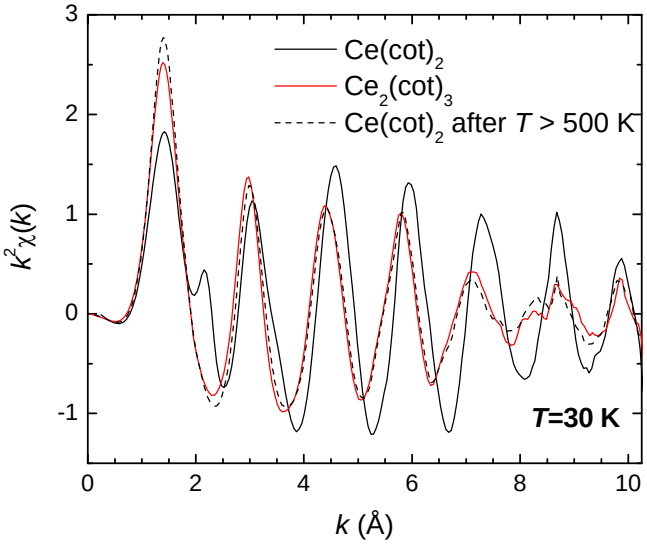

Figure 8. The EXAFS function $k^2\chi(k)$ vs. k for the same samples as in Figure 7. The EXAFS for $Ce_2(cot)_3$ and the $Ce(cot)_2$ sample after heating to 500 K are nearly identical.

Systematic errors in EXAFS bond lengths are often quoted as 0.005 Å for the nearest neighbors, larger for further neighbors, and similarly the nearest neighbor σ^2 errors are about 10%. These estimates have been made by direct comparisons to standard crystalline materials,[44] and vary somewhat with the atomic number Z. Hydrogen, however, is a largely unexplored case. We therefore expect that systematic errors in this scattering shell in the fit may be substantially larger that in the other scattering shells.

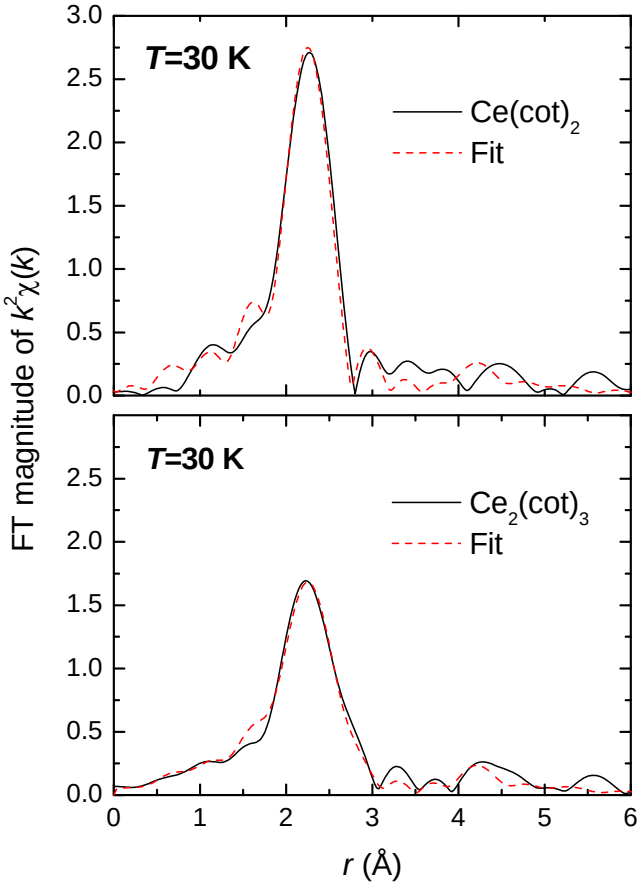

Figure 9. Fourier transforms (FT) of $k^2\chi(k)$ data in Figure 8, transformed between 2.5 and 10.3 Å^{-1}, and Gaussian narrowed by 0.3 Å^{-1}. The data and fit of $Ce_2(cot)_3$ that was heated to 500 K and then cooled to 30 K are nearly identical to those from $Ce_2(cot)_3$ data, and so are not shown for clarity (see Figure 7).

The final results in Table 2 and Figure 9 indicate that the 16 nearest-neighbors carbons to Ce are at 2.68 Å and have a narrow σ^2. For comparison, Table 3 lists structural information on $Ce(cot)_2$ and related compounds obtained from single crystal X-ray diffraction experiments. S_0^2 is allowed to vary in these fits, and we obtain a value of 0.8. A similar quality fit is obtained for $Ce_2(cot)_3$, except that the Ce-C distance is 2.73(1) Å, and that pair's σ^2 is much wider. This result is expected in a triple-decker molecule, as the middle cot ring should be more loosely bound than the outer cot rings. The size of the shift in bond length and the magnitude of the increased pair-distance variance are both consistent with a

2.68 Å distance from the Ce to the outer cot carbons and a 2.78 Å distance to the inner cot carbons. Interestingly, the Ce-H contribution near 3 Å is necessary to fit the high-*r* shoulder on the main Ce-C peak in the Fourier transforms. It is rare in EXAFS analysis that hydrogen has a large enough relative scattering amplitude to be required in a fit, but since this Ce-H shell has 16 hydrogens at nearly the same distance, they combine to form an important contribution (their presence is confirmed by a Hamilton-test).[45]

Table 2. Fit results from Ce L_{III}-edge EXAFS data for $Ce(cot)_2$ and $Ce_2(cot)_3$ samples. Overall scale factors are measured to be 0.84(13) and 0.80(8), and threshold energy shifts ΔE_0=-7.7(10) eV and –5.6(8) eV, respectively. Reported errors for EXAFS results are determined by a Monte Carlo method. Data are transformed as in Figure 6 and are fit between 1.2 and 5.0 Å. Multiple scattering shells are included in the fit.

	$Ce(cot)_2$			$Ce_2(cot)_3$		
	N	R(Å)	σ^2(Å^2)	N	R(Å)	σ^2(Å^2)
Ce-C	16	2.68(1)	0.001(1)	16	2.73(1)	0.007(1)
Ce-H	16	2.93(6)	0.0001(1)	16	3.10(3)	0.0001(1)
Ce-Ce				1	4.04(5)	0.006(6)

Table 3. Selected Bond Distances (Å) and Angles (°) for $[Li(thf)_4][Ce(C_8H_8)_2]$, $Ce(C_8H_8)_2$ and $Ce(MeC_8H_7)_2$ and $[1,3,6\text{-}(Me_3Si)_3C_8H_5]_2Ce$.

Compound	$[Li(thf)_4][Ce(C_8H_8)_2]$ [a]	$Ce(C_8H_8)_2$ [b]	$Ce(MeC_8H_7)_2$ [c]	$[1,3,6\text{-}(Me_3Si)_3C_8H_5]_2Ce$ [d]
Ce-C (mean)	2.74(1)	2.674(5)	2.692(6)	2.704(7)
Ce-Cent	2.04	1.97	1.97	1.98
Cent-Ce-Cent	180	180	176	176

[a] ref. 14, [b] ref. 28, [c] ref. 46, [d] ref. 47

As discussed above for the Ce L_{III} XANES data, the $Ce(cot)_2$ sample was heated to approximately 500 K and then cooled to 30 K, where we remeasured the EXAFS. Figure 8 shows that the local structure around Ce in the heated sample of $Ce(cot)_2$ is practically identical with the authentic $Ce_2(cot)_3$, a result that is consistent with the melting experiment described above.

To summarize the X-ray absorption results, $Ce(cot)_2$ is found to have an f-occupancy n_f=0.89, while cerium in $Ce_2(cot)_3$ is trivalent and n_f=1. The local structure around cerium in cerocene is consistent with that found in the crystal structure (Table 2 and 3), including the surprising result that the Ce-H near neighbors must be included in the fitting model to obtain fits of reasonable quality. The local cerium structure in $Ce_2(cot)_3$ indicates a broadened and lengthened Ce-C pair-distance distribution, consistent with the nominal triple-decker model where Ce-C distances are 0.1 Å longer toward the inner cot ring than the outer cot rings.

The Kondo Model applied to Cerocene. The original calculational result suggesting that the ground state of cerocene is not identical to that of the isoelectronic thorocene, $Th(cot)_2$, as inferred from Xα calculations[48] and PES data[3] was published by Neumann and Fulde.[5] This calculation makes the provocative claim that the ground state configuration of cerocene is $[Ce(III, f^1(e_{2u}^1)][(COT^{-1.5})_2 (e_{2u}^3)]$, which is an open-shell orbital singlet of $^1A_{1g}$ symmetry (in D_{8h} symmetry) and is therefore non-magnetic. This configuration is lowered in energy relative to the triplet state ($^3E_{2g}$) due to configuration interaction with the closed-shell configuration, $[Ce(IV) f^0(e_{2u}^0)][(COT^{-2})_2(e_{2u}^4)]$ also of $^1A_{1g}$ symmetry. Multireference configuration interaction including single and double excitation (MRCISD) calculations are fully consistent with the original calculational results, but extends and amplifies them.[6-8] Thus, the currently accepted calculational model of the ground state configuration of cerocene is an admixture of the two $^1A_{1g}$ configurations $[Ce(III, f^1(e_{2u}^1)][(cot^{-1.5})_2(e_{2u}^3)]$ and $[Ce(IV) f^0(e_{2u}^0)][(cot^{-2})_2(e_{2u}^4)]$ in an approximate ratio of 80:20, respectively. These calculational results are fully consistent with the

experimental data derived from XANES and magnetic susceptibility studies as a function of temperature.[12] The L_{III} edge XANES data show signatures for the Ce(III) and Ce(IV) wave functions and the relative populations are approximate 90:10, respectively, in agreement with calculation. The magnetic susceptibility data show that cerocene is a temperature independent paramagnet (TIP) to 300 K, also consistent with calculation.

The original notion advanced by Neumann and Fulde, viz., that cerocene is a molecular analogue of a Kondo singlet, is a model that is unfamiliar to molecular chemists.[49] The Kondo model has been used by solid state physicists to rationalize the experimental facts that certain metal alloys, for example $CeAl_3$, are ground state singlets with a mixed-configuration ground state. Using language that is more familiar to molecular chemists, the Kondo singlet is synonymous with an open-shell singlet (S = 0) that is lower in energy than the open-shell triplet as a result of an admixture of the two configurations [Ce(III, $f^1(e_{2u}{}^1)$][$(cot^{-1.5})_2$ $(e_{2u}{}^3)$] and [Ce(IV), $f^0(e_{2u}{}^0)$][$(cot^{-2})_2(e_{2u}{}^4)$]. Thus, the term Kondo singlet means that the ground state is a multiconfigurational open-shell singlet state. As the temperature of the system is increased, the triplet state becomes populated, and at higher temperature (the Kondo temperature) the spins become uncorrelated. Clearly cerocene behaves as a Kondo singlet to 300 K but decomposes to $Ce_2(cot)_3$ and COT before the triplet state becomes populated.

Recently, gas-phase photoelectron spectra for $(C_5H_5)_3Ce$,[50] and L_{III} edge X-ray absorption spectroscopy and magnetic susceptibility studies, as a function of temperature, have been reported for bis(hexamethylpentalene)cerium, $(Me_6C_8)_2Ce$.[51] These data are consistent with a model that these organometallic compounds have a multiconfigurational ground state, similar to that found in cerocene. More recently, similar spectroscopic studies were reported on the tri-*i*-propylsilyl analogue, (1,4-(*i*-$Pr_3Si)_2C_8H_4)_2Ce$, and related derivatives.[52] These authors, however, advance the proposition that "it seems appropriate to retain the formal description of these multiconfigurational ground state species as Ce(IV)", a proposition with which we disagree. Clearly, the configuration that dominates in cerocene is [Ce(III, $f^1(e_{2u}{}^1)$][$(cot^{-1.5})_2$ $(e_{2u}{}^3)$], and therefore we advocate the view that these organometallic molecules are thought of as open-shell singlet molecules in which the oxidation number of cerium is

ambiguous and they are representatives of intermediate valence compounds using the term as defined by the physics community.[53]

Epilog

In this work, $[Li(thf)_4][Ce(cot)_2]$, $Ce(cot)_2$ and $Ce_2(cot)_3$ have been synthesized by reproducible synthetic procedures in moderate to good yield and high purity. $Ce(cot)_2$ is synthesized by oxidizing the anion, $[Ce(cot)_2]^-$, with ferrocenium salts or *p*-benzoquinone. Cerocene is less thermally stable than either thorocene or uranocene, since in the solid state, it eliminates C_8H_8 on heating to give $Ce_2(cot)_3$. On the synthetic scale, this is an excellent route to the Ce(III) triple-decker complex, $[Ce(III)]_2[(cot)^{2-}]_3$. This thermal process was verified by Ce L_{III} EXAFS and XANES experiments on solid state samples. The Ce-C distance in $Ce_2(cot)_3$ derived from EXAFS increases to 2.74 Å, compared to the Ce-C distance of 2.69 Å for $Ce(cot)_2$.

The experimental data reported in this article and in an earlier one[12] and calculational results reported even earlier,[8] agree that the electronic structure of cerocene is multiconfigurational begets the question of why its electronic structure is so different from that of thorocene, $Th(cot)_2$, which is described by a single configuration wave function [Th(IV), $f^0(e_{2u}{}^0)][(cot^{-2})_2(e_{2u}{}^4)]$.[8] The physical properties of thorocene have been summarized,[29, 31] but the key electronic structure data are that $Th(cot)_2$ is diamagnetic, $\chi_m = -2.0(1) \times 10^{-4}$ cm^3 mol^{-1}, over the temperature range 26-300 K, and the calculation shows that it is a closed-shell singlet of $^1A_{1g}$ symmetry. A Mulliken population analysis of the SCF wave function shows that the 5f and 6d orbitals play a significant role in the thorium to ring bonding, which is consistent with early PES data.[4] Thus, the ground state electronic structure is "normal", which makes the electronic structure of cerocene so very unusual and fascinating. The differences may be traced to the relative energy of the electrons in the 4f and 5f shell and how the different metals deal with the requirements of the Pauling electroneutrality principle.[54]

The energy difference between the experimental 4th ionization energy for the free ions in the gas phase for $Ce^{3+/4+}{}_{(g)}$ and $Th^{3+/4+}{}_{(g)}$ is 36.8 eV and 28.8 eV, respectively.[55, 56] Thus, the $5f^1$ electron is

destabilized relative to the $4f^1$ electron by about 8 eV, *i.e.*, the $4f^1$ electron is a core electron, a result that is consistent with the larger relativistic effects on the nuclei with larger values of Z, which destabilizes the 5f and 6d shells.[6, 57] One ramification of this is that the energy involved in making $M(IV)(cot^{-2})_2$, with a $f^0(e_{2u}{}^0)$ $(cot^{-2})_2(e_{2u}{}^4)$ configuration requires less energy for thorium than for cerium. In $Th(cot)_2$ the enthalpy penalty is compensated by transfer of electron density from $e_{2u}{}^4$ and $e_{2g}{}^4$ ligand molecular orbitals to thorium by way of the 6f and 5d atomic orbitals, respectively, so that the charge on thorium is not +4. A Mulliken population analysis on the SCF wave functions estimates that the charge on thorium is +1.2, i.e. $Th(cot)_2$ is covalent: it shares its valences in order to reduce the charge on the metal. Cerium in $Ce(cot)_2$, however, does not share its valence as readily; the Mulliken population analysis estimates that the charge on cerium is +1.8 in the multiconfigurational wave function, in which the Ce(III):Ce(IV) configurations are weighted 80:20.[8] The difference in charge density at the metal may be thought of as a way in which these two metals in $M(cot)_2$ deal with the restrictions of the Pauling electroneutrality principle. In the case of M = Th, the net charge density on the metal is reduced by covalent bonding. When M = Ce, the reduced covalence within the requirement of the electroneutrality principle means that the [Ce(III), $f^1(e_{2u}{}^1)$][$(cot^{-1.5})_2$ $(e_{2u}{}^3)$] structure must dominate the [Ce(IV), $f^0(e_{2u}{}^0)$][$(cot^{-2})_2(e_{2u}{}^4)$] structure, in valence bond language, which is equivalent to the molecular orbital language used above. In this manner, the abnormal behavior of cerocene, relative to thorocene, may be explained in language that is familiar to molecular chemists.

The proposed mechanism for the multiconfigurational ground state is a lowering of the Ce(III, $4f^1)(cot^{1.5-})_2$ configuration energy due to an antiferromagnetic interaction between the local f^1 orbital hybridized with the π electrons on the COT ring. This mechanism should not be unique to cerocene, and may be an important component for understanding chemical bonding and magnetism in a very wide range of molecular organometallic compounds. The extension of the concept of multiconfigurational ground states to other 4f-block metal compounds will bring this topic, which is currently in the domain of physicists, into the chemistry community. One such extension is to Yb(II) compounds, as mentioned by Neumann und Fulde;[5] a specific example is the magnetic behavior of $(C_5Me_5)_2Yb(bipy)$.[12] These

concepts are controversial despite the above calculations and measurements;[6-9, 12] however, cerocene stands apart from these other materials because of its high symmetry (D_{8h}), which makes the high-level CI calculations manageable, and because of cerocene's status as the first molecule where the multiconfigurational interaction concept has been seriously considered.

Experimental Section

General Comments. All reactions, product manipulations and characterizations have been carried out as previously described.[19, 58] Magnetic measurements were conducted in a 7 T Quantum Design MPMS magnetometer utilizing a superconducting quantum interference device (SQUID). Between 10 and 25 mg of sample were sealed in evacuated quartz tubes while held in place with ~5 mg of quartz wool. This method provided a very small and reliable container correction, typically of about -2×10^{-5} emu/mol. The data were also corrected for the overall diamagnetism of the molecule using Pascal constants.[59] For a more detailed description see ref. 19. Electron paramagnetic resonance (EPR) spectra were obtained with a Varian E-12 spectrometer equipped with an Oxford ESR10 continuous flow helium cryostat, an EIP-547 microwave frequency counter, and a Varian E-500 gaussmeter, which was calibrated using 2,2-diphenyl-1-picrylhydrazyl (DPPH, g = 2.0036). The EPR sample space was continuously pumped, and temperature was controlled by changing the pressure in the sample space. The temperature was recorded using a thermocouple in the cold He stream just below the sample space, and the actual temperature of the sample is assumed to be slightly greater. The low temperature spectra were fit using a version of the code ABVG modified to fit spectra in the frequency regime as suggested by Pilbrow and to fit spectra using the Levenberg-Marquardt method.[60-62]

$Li_2(C_8H_8)(thf)_{1.7}$.[63] Cyclooctatetraene (3.8 mL, 3.52 g, 32.5 mmol) was added to lithium wire (0.46 g, 66.2 mmol), cut into small pieces, in 50 mL of tetrahydrofuran at room temperature. The reaction mixture became warm, and changed color to brown, then green while it was stirred overnight at room temperature. The solution was filtered, concentrated to ca. 30 mL and cooled to -25 °C. Two crops of

light green crystals were isolated and exposed to dynamic vacuum for 2 hours at room temperature. During this desolvation process the crystals collapsed to a grey-yellow powder that still contained coordinated tetrahydrofuran, $Li_2(C_8H_8)(thf)_{1.7}$ (4.38 g, 18.2 mmol, 56 %). The tetrahydrofuran content was established by ^{1}H NMR spectroscopy in pyridine-d_5. Warning: Dry sodium and potassium salts of cyclooctatetraene react explosively with air, whereas the lithium salt is less reactive with air, but it must be handled with care. The lithium salt can be stored at room temperature in a well-sealed Schlenk tube under a nitrogen atmosphere.

$[Li(thf)_4][Ce(C_8H_8)_2]$.[14] $Li_2(C_8H_8)(thf)_{1.7}$ (2.95 g, 12.3 mmol) and anhydrous $CeCl_3$ (1.51 g, 6.15 mmol) were weighed into a Schlenk flask under nitrogen, suspended in tetrahydrofuran (60 mL) and stirred at reflux overnight. During this time the color changed to lime green and the suspension was allowed to cool to room temperature. The deep green tetrahydrofuran solution was filtered through a glass fiber filter, concentrated to ca. 40 mL and cooled to –20 °C. Two crops of light green needles were isolated (2.62 g, 4.07 mmol, 66 %). The crystals obtained were exceedingly sensitive to moisture and air. Even trace amounts of oxygen caused a significant color change to deep red, before turning yellow. The dark red compound was identified as $Ce(C_8H_8)_2$ by ^{1}H NMR spectroscopy. The crystals lost coordinated tetrahydrofuran at elevated temperature on exposure to dynamic vacuum; the tetrahydrofuran content was established either by integration of the ^{1}H NMR spectrum in pyridine-d_5 or after hydrolysis of a sample with D_2O in C_6D_6. M.p. 330 °C (dec.). ^{1}H NMR (C_5D_5N, 20 °C): δ 3.66 (16H, t, $^3J_{CH}$ = 6.0 Hz, α-CH_2), 2.44 (16H, $\nu_{1/2}$ = 130 Hz, C_8H_8), 1.61 (16H, $^3J_{CH}$ = 6.0 Hz, β-CH_2). ^{1}H NMR (C_4D_8O, 20 °C): δ 3.60 (16H, br. s, α-CH_2), 1.66 (16H, br. s, β-CH_2), 1.50 (16H, $\nu_{1/2}$ = 100 Hz, C_8H_8). IR (Nujol mull; CsI windows; cm^{-1}): 1815 (br. w), 1700 (w), 1580 (br. w), 1555 (br. vw), 1341 (m) 1305 (vw), 1260 (vw), 1180 (vbr. w), 1200 (sh), 1045 (vs), 920 (m), 895 (vs), 800 (vw), 762 (m), 740 (m), 722 (sh), 701 (m), 681 (vs), 610 (vw), 470 (sh), 425 (br. m), 370 (sh), 340 (br. s), 232 (vs).

[Ce(C_8H_8)$_2$].][Li(thf)$_4$][Ce(C_8H_8)$_2$] (2.57 g, 4.0 mmol) was exposed at 100 °C to dynamic vacuum for 2 hours to ensure the complete removal of the coordinated tetrahydrofuran. During desolvation the green crystals collapsed to a fine green powder. Freshly sublimed *p*-benzoquinone (0.43 g, 4.0 mmol) was added; even in the solid state an immediate color change to brown-purple was observed. Toluene (40 mL) was added and the suspension was stirred at 80 °C for 1 h, then the solvent was slowly removed under dynamic vacuum. The residue was placed into an extraction frit and the material was continuously extracted with boiling toluene for 12 hours, at which time the toluene extracts were colorless. The deep red toluene extracts were allowed to cool slowly to room temperature, during which time deep red crystals formed. The mother liquor was separated from the crystals by filtration and cooled to –25 °C to yield a second crop of red needles (0.80 g, 2.30 mmol, 58 %). M.p. 290 °C (dec.). The absence of lithium containing by-products was verified by a negative flame test. In the solid state it inflamed in air. ^{1}H NMR (C_6D_6, 20°C): δ 5.79 ($\nu_{1/2}$ = 2.4 Hz). ^{13}C{^{1}H} NMR (C_6D_6, 20°C): δ 114.9. The E.I. mass spectrum showed a molecular ion at m/e= 348 amu. The parent ion isotopic cluster was simulated: (calcd. %, observd. %): 348 (100,100), 349 (18,17), 350 (14,14), 351 (2,2). IR (Nujol mull; CsI windows; cm^{-1}): 1880 (vw), 1780 (vw), 1318 (m), 1260 (vw), 1162 (vw), 1098 (vw), 898 (s), 785 (m), 742 (s), 730 (sh. m), 688 (vs), 249 (s).

[Ce_2(C_8H_8)$_3$]. Ce(C_8H_8)$_2$ (0.25 g, 0.72 mmol) was placed into a Schlenk tube, exposed to dynamic vacuum and then heated to 300 °C over a period of 15 min. During this time the color changed from dark red to light green and the crystals collapsed to a light green powder (0.2 g, 0.34 mmol, 94 %). M.p. > 340 °C. The light green material was insoluble in aromatic hydrocarbons, and the IR spectrum was identical to that reported.[1] IR (Nujol mull; CsI windows; cm^{-1}): 1880 (vw), 1838 (vw), 1772 (vw), 1728 (vw), 1580 (vw), 1427 (m), 1312 (m), 1262 (m), 898 (s), 850 (sh), 845 (w), 800 (m), 742 (s), 728 (s), 695 (vs), 682 (vs), 240 (sh), 232 (vs), 210 (s). In an NMR tube, $Ce_2(C_8H_8)_3$ was suspended in C_6D_6 and an excess of C_8H_8 was added and the NMR tube was heated at 65 °C. Over a period of 4 months the

quantity of $Ce(C_8H_8)_2$ increased steadily, as the green solid, $Ce_2(C_8H_8)_3$, dissolved and the C_6D_6 solution turned deep red.

EXAFS/XANES Experiments. In order to perform X-ray absorption measurements on these air and moisture sensitive samples, an aluminum sample holder out of aluminum with machined slots was designed. X-ray windows are pressed onto this holder body with an intervening lead or indium wire seal. Although aluminized mylar windows worked well for protecting the samples from oxygen, for this study pinhole-free 0.001 inch-thick aluminum windows were used. Such windows allowed for heating the samples above 500 K while still allowing a reasonable transmission of X-rays. Samples were placed in an argon-filled inert atmosphere glove box, ground, mixed with dry boron nitride, packed into the holder slots and sealed. These holders were placed in argon-filled containers, which were not opened until it was time to load the holders into the liquid helium flow cryostat at the Stanford Synchrotron Radiation Laboratory (SSRL). The holder exteriors were exposed to air for a few minutes while they were loaded into the cryostat, which was then evacuated, flushing several times with He gas. In any case, these holders have been shown to be robust enough to suffer exposure to air for much longer periods of time before the sample is compromised. Data were collected on BL 10-2 at SSRL using a double Si(111) crystal monochromator to reject the second harmonic energy. Higher-order harmonics were rejected by detuning the second crystal by about 50%. Data were collected in transmission mode at T=30 K, and the change in absorption at the Ce L_{III} edge corresponds to about 0.7 absorption lengths. Samples of $Ce(cot)_2$ and $Ce_2(cot)_3$ were measured, in addition to repeating the measurement on $Ce(cot)_2$ after transforming the sample by heating above 500 K. Data reduction and fitting procedures follow standard procedures.[44] In particular, the absorption threshold E_0 was estimated by taking the energy at the half-height of the edge, and the photoelectron wave vector k was then calculated from $\hbar^2k^2=2m_e(E-E_0)$, where E is the incident photon energy and m_e is the electron rest mass. The EXAFS oscillations $\chi(k)$ are then extracted by subtracting the so-called embedded atom absorption $\mu_0(k)$ and normalizing by it: $\chi(k)=(\mu(k)-\mu_0(k))/\mu_0(k)$.These k-space data are then Fourier transformed into r-space. Peaks in the

Fourier transforms (FT's) generally correspond to neighboring scattering shells. Actual bond lengths are shifted on the measured *r*-axis by phase shifts of the photoelectron at the absorbing and backscattering atoms, and the scattering amplitudes are complicated functions of *k* and *r*. These functions are calculated by the FEFF7 code,[64] and actual structural information is obtained by using these calculated function in fits to the EXAFS data. These fits are performed in *r*-space using the RSXAP fitting package.[65, 66] Error estimates use a Monte Carlo technique.

Acknowledgement. This work was supported by the Director, Office of Science, Office of Basic Energy Sciences, of the U.S. Department of Energy under Contract No. DE-AC02-05CH11231. We thank Norman Edelstein for helpful discussions about the electronic structure of lanthanides and the German Academic Exchange Service (DAAD) for a fellowship (M.D.W.). XANES and EXAFS data were collected at the SSRL, a national user facility operated by Stanford University on behalf of the DOE/OBES.

Supporting Information Available. Details on the Calculation of g-values for Ce(III) including orbital reduction factor, variable temperature EPR spectra of $Ce_2(cot)_3$ and variable temperature Ce L_{III} edge XANES spectra of $Ce(cot)_2$. This material is available free of charge via the Internet at http://pubs.acs.org.

References

[1] Greco, A.; Cesca, S.; Bertolini, G., *J. Organomet. Chem.* **1976,** *113*, 321-330.

[2] Avdeef, A.; Raymond, K. N.; Hodgson, K. O.; Zalkin, A., *Inorg. Chem.* **1972,** *11*, 1083-1088.

[3] Streitwieser, A.; Kinsley, S. A.; Rigsbee, J. T.; Fragala, I. L.; Ciliberto, E.; Rosch, N., *J. Am. Chem. Soc.* **1985,** *107*, 7786-7788.

[4] Clark, J. P.; Green, J. C., *J. Chem. Soc., Dalton Trans.* **1977**, 305.

[5] Neumann, C.-S.; Fulde, P., *Z. Physik B* **1989,** *74*, 277-278.

[6] Dolg, M.; Fulde, P., *Chem. Eur. J.* **1998,** *4*, 200-204.

[7] Dolg, M.; Fulde, P.; Kuchle, W.; Neumann, C. S.; Stoll, H., *J. Chem. Phys.* **1991,** *94*, 3011-3017.

[8] Dolg, M.; Fulde, P.; Stoll, H.; Preuss, H.; Chang, A.; Pitzer, R. M., *Chem. Phys.* **1995,** *195*, 71-82.

[9] Dolg, M.; Stoll, H., Electronic Structure Calculations for Molecules Containing Lanthanide Atoms. In *Handbook of Chemistry and Physics of Rare Earths*, ed.; Gschneider, K. A.; Eyring, L., Eds. Elsevier: Amsterdam, 1996; Vol. 22, pp 607-729.

[10] Edelstein, N. M.; Allen, P. G.; Bucher, J. J.; Shuh, D. K.; Sofield, C. D.; Kaltsoyannis, N.; Maunder, G. H.; Russo, M. R.; Sella, A., *J. Am. Chem. Soc.* **1996,** *118*, 13115-13116.

[11] Amberger, H.-D.; Reddmann, H.; Edelmann, F. T., *J. Organomet. Chem.* **2005,** *690*, 2238-2242.

[12] Booth, C. H.; Walter, M. D.; Daniel, M.; Lukens, W. W.; Andersen, R. A., *Phys. Rev. Lett.* **2005,** *95*, 267202.

[13] Hodgson, K. O.; Mares, F.; Starks, D. F.; Streitwieser, A., *J. Am. Chem. Soc.* **1973,** *95*, 8650-8658.

[14] Kilimann, U.; Schäfer, M.; Herbst-Irmer, R.; Edelmann, F. T., *J. Organomet. Chem.* **1994,** *469*, C15-C18.

[15] Streitwieser, A.; Kinsley, S. A.; Jenson, C. H.; Rigsbee, J. T., *Organometallics* **2004,** *23*, 5169-5175.

[16] Warren, K. D., *Inorg. Chem.* **1975,** *14*, 3095-3103.

[17] Warren, K. D., *Struct. Bond.* **1977,** *33*, 97-138.

[18] Clack, D. W.; Warren, K. D., *J. Organomet. Chem.* **1976,** *122*, C28-C30.

[19] Walter, M. D.; Schultz, M.; Andersen, R. A., *New J. Chem.* **2006,** *30*, 238-246.

[20] Abragam, A.; Bleaney, B., *Electron Paramagnetic Resonance of Transition Ions*.; Clarendon Press: Oxford, 1970.

[21] Judd, B. R., *Proc. Roy. Soc.* **1955,** *232A*, 458-474.

[22] Gourier, D.; Courant, D.; Arliguie, T.; Ephritikhine, M., *J. Am. Chem. Soc.* **1998,** *1998*, 6084-6092.

[23] In control experiments it has been demonstrated that $Ce(C_8H_8)_2$ does not react with Cp_2Fe.

[24] Walter, M. D.; Fandos, R.; Andersen, R. A., *New J. Chem.* **2006,** *30*, 1065-1070.

[25] Interestingly, during the extraction process of cerocene with hot toluene (b.p. 110 °C), a small amount of $Ce_2(C_8H_8)_3$ is formed and to obtain cerocene in absolute pure form, it is necessary to recrystallize the contaminated material from toluene at -20 °C.

[26] Streitwieser, A.; Müller-Westerhoff, U.; Sonnichsen, G.; Mares, F.; Morrell, D. G.; Hodgson, K. O.; Harmon, C. A., *J. Am. Chem. Soc.* **1973,** *95*, 8644-8649.

[27] Streitwieser, A.; Yoshida, N., *J. Am. Chem. Soc.* **1969,** *91*, 7528.

[28] Kurras, E.; Krüger, C., Private Communication to the Cambridge Structural Database, deposit number CCDC 256935. 2004.

[29] *Gmelin Handbook of Inorganic Chemistry, Thorium, Supplement Volume E, Coordination Compounds*. ed.; Springer: Berlin, 1985; p 256.

[30] Goffart, J.; Fuger, J.; Gilbert, B.; Kanellakopulos, B.; Duyckaerts, G., *Inorg. Nucl. Chem. Lett.* **1972,** *8*, 403-412.

[31] $Th(cot)_2$ decomposes at 190 °C without melting. *Gmelin Handbook of Inorganic Chemistry,Thorium, Supplement Volume E,Coordination Chemistry*. ed.; Springer: Berlin, 1985, p. 258.

[32] Streitwieser, A.; Müller-Westerhoff, U.; Mares, F.; Grant, C. B.; Morrell, D. G., *Inorg. Synth.* **1979,** *19*, 149-154.

[33] *Gmelin Handbuch der Anorganischen Chemie, Uranium, Supplement Volume E2, Coordination Compounds*. ed.; Springer: Berlin, 1980.

[34] Wilke, G.; Breil, H., *Angew. Chem. Int. Ed. Engl.* **1966,** *5*, 898-899.

[35] DeKock, C. W.; Ely, S. R.; Hopkins, T. E.; Brault, M. A., *Inorg. Chem.* **1978,** *17*, 625-631.

[36] Bencini, A.; Gatteschi, D., *EPR of Exchange Coupled Systems.* Springer-Verlag: New York, 1990.

[37] Lines, M. E., *J. Chem. Phys.* **1971,** *55*, 2977-2984.

[38] Kahn, O., *Molecular Magnetism*. VCH: New York, 1993.

[39] Berg, D. J.; Boncella, J. M.; Andersen, R. A., *Organometallics* **2002,** *21*, 4622-4631.

[40] Rosen, R. K.; Andersen, R. A.; Edelstein, N. M., *J. Am. Chem. Soc.* **1990,** *112*, 4588-4590.

[41] Kaindl, G.; Wertheim, G. K.; Schmiester, G.; Sampathkumaran, E. V., *Phys. Rev. Lett.* **1987,** *58*, 606.

[42] Kaindl, G.; Schmiester, G.; Sampathkumaran, E. V.; Wachter, P., *Phys. Rev. B* **1988,** *38*, 10174-10177.

[43] Kotani, A.; Jo, T.; Parlebas, J. C., *Adv. Phys.* **1988,** *37*, 37-85.

[44] Li, G. G.; Bridges, F.; Booth, C. H., *Phys. Rev. B* **1995,** *52*, 6332-6348.

[45] Klementev, K. V., *Nucl. Instr. and Meth. A* **2001,** *470*, 310-314.

[46] Boussie, T. R.; Eisenberg, D. C.; Rigsbee, J.; Streitwieser, A.; Zalkin, A., *Organometallics* **1991,** *10*, 1022-1028.

[47] Kilimann, U.; Herbst-Irmer, R.; Stalke, D.; Edelmann, F. T., *Angew. Chem.* **1994,** *106*, 1684-1687; *Angew. Chem. Int. Ed. Engl.* **1994**, *33*, 1618-1621.

[48] Roesch, N.; Streitwieser, A., *J. Am. Chem. Soc.* **1983,** *105*, 7237-7240.

[49] Fulde, P., *J. Phys. F: Met. Phys.* **1988,** *18*, 601-639.

[50] Coreno, M.; de Simone, M.; Green, J. C.; Kaltsoyannis, N.; Narband, N.; Sella, A., *Chem. Phys. Lett.* **2006,** *432*, 17-21.

[51] Ashley, A.; Balazs, G.; Cowley, A.; Green, J. C.; Booth, C. H.; O'Hare, D., *Chem. Commun.* **2007**, 1515-1517.

[52] Balazs, G.; Cloke, F. G. N.; Green, J. C.; Harker, R. M.; Harrison, A.; Hitchcock, P. B.; Jardine, C. N.; Walton, R., *Organometallics* **2007,** *26*, 3111-3119.

[53] LaBute, M. X.; Kulkarni, R. V.; Endres, R. G.; Cox, D. L., *J. Chem. Phys.* **2002,** *116*, 3681-3689.

[54] Pauling, L., *The Nature of the Chemical Bond*. Cornell University Press: Ithaca, NY, 1960; 'Vol.' p 172 and 270.

[55] Martin, W. C.; Hagan, L.; Reader, J.; Sugar, J., *J. Phys. Chem. Ref. Data* **1974,** *3*, 771.

[56] Sugar, J., *J. Opt. Soc. Am.* **1975,** *65*, 1366.

[57] Pyykkö, P., *Chem. Rev.* **1988,** *88*, 563-594.

[58] Schultz, M.; Boncella, J. M.; Berg, D. J.; Tilley, T. D.; Andersen, R. A., *Organometallics* **2002,** *21*, 460-472.

[59] O'Connor, C. J., *Prog. Inorg. Chem.* **1982,** *29*, 203-285.

[60] Daul, C.; Schlapfer, C. W.; Mohos, B.; Ammeter, J.; Gamp, E., *Comp. Phys. Commun.* **1981,** *21*, 385-395.

[61] Pilbrow, J. R., *Transition Ion Electron Paramagnetic Resonance.*; Oxford University Press: New York, 1990.

[62] Press, W. H.; Teukolsky, S. A.; Vetterling, W. T.; Flannery, B. P., *Numerical Recipes in Fortran 77*. Second Edition; Cambridge University Press: New York, 1992.

[63] Strauss, H. L.; Katz, T. J.; Fraenkel, G. K., *J. Am. Chem. Soc.* **1963,** *85*, 2360-2364.

[64] Ankudinov, A. L.; Rehr, J. J., *Theory. Phys. Rev. B* **1997,** *56*, R1712-R1716.

[65] Real Space X-ray Absorption Package. http://lise.lbl.gov/RSXAP/.

[66] Hayes, T. M.; Boyce, J. B., *Extended x-ray absorption fine structure spectroscopy*. ed.; Academic: New York, 1982; Vol. 37, pp 173-351.

For Table of Contents (TOC) only:

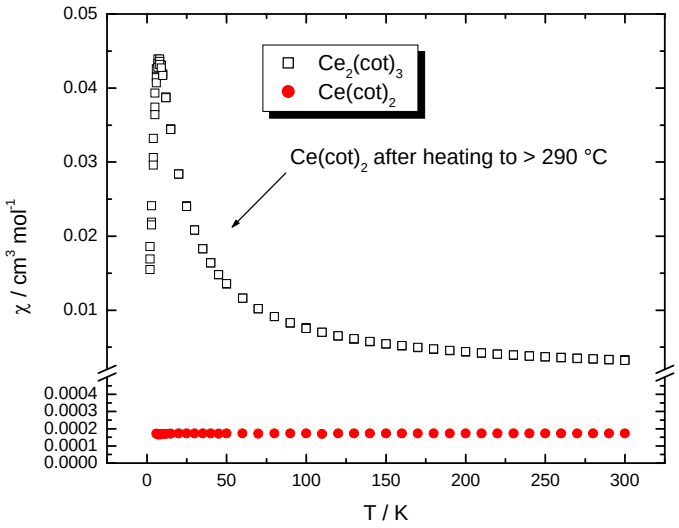

$Ce(cot)_2$ is not diamagnetic, but a temperature independent paramagnet. The individual spin carriers, Ce(III, f^1) in $Ce_2(cot)_3$ are correlated below 10 K, but uncorrelated at higher temperatures.